Hindawi
Advances in Civil Engineering
Volume 2024, Article ID 7970436, 17 pages
https://doi.org/10.1155/2024/7970436

Research Article

Near-Fault Response and Loading Protocols of Box Columns in Steel Frames with Self-Centering Braces to Provide Recentering Capability

Yu-Fang Liu,[1] **Chung-Che Chou**,[1,2] **Chia-Ying Chung**,[2] **and Hao-Che Huang**[2]

[1]*National Center for Research on Earthquake Engineering, Taipei, Taiwan*
[2]*Department of Civil Engineering, National Taiwan University, Taipei, Taiwan*

Correspondence should be addressed to Chung-Che Chou; cechou@ntu.edu.tw

Received 29 May 2023; Revised 5 October 2023; Accepted 14 December 2023; Published 11 January 2024

Academic Editor: John Mander

The main objective of this study was to establish loading protocols for self-centering braced frames (SCBFs) while taking into account the impact of near-fault ground motions. SCBFs are self-centering frames that have lower residual drift than buckling-restrained braced frames (BRBFs) under near-fault earthquakes; thus, SCBFs can better control damage to buildings. Typically, first-story columns are employed to represent the seismic behavior of a structure; therefore, loading protocols were developed for first-story columns in SCBFs under near-fault earthquakes. Nonlinear static and dynamic analyses of SCBFs designed with various periods were conducted for better understanding the seismic performance of SCBFs. Finally, the loading protocols developed for SCBFs were compared with those for BRBFs under the same near-fault motions.

1. Introduction

Current design practices for steel high-rise buildings typically employ braces to withstand seismic forces. These brace systems, typically named as eccentrically braced frames (EBFs), concentrically braced frames (CRFs), or buckling-restrained braced frames (BRBFs), can enhance the strength and stiffness of the buildings effectively. Liu et al. [1] conducted a nonlinear analysis for BRBFs and developed loading protocols for these frames under near-fault earthquakes. It was found that the loading protocol for the story drift in BRBFs has a permanent residual drift due to pulse-type earthquakes.

The current study investigates a dual frame system, which is composed of special moment frames (SMFs) and the self-centering braced frames (SCBFs) to resist seismic forces and reduce residual drift [2, 3]. While the AISC 341-16 [4] lacks a lateral displacement loading protocol for testing a column. In general, near-fault ground motions alter in residual and story drifts of buildings. In order to comprehend the impact of near-fault earthquakes on the seismic response of buildings, it is necessary to assess the variation of axial force and story drift for columns since the column near the base in the first floor is allowed to form a plastic hinge.

Four buildings were designed in this work to simulate structures with varying structural periods. Observing the actual dynamic behavior of high-rise buildings through nonlinear static analysis of frames is difficult due to the greater influence of higher mode effects when compared to low-to-medium rise buildings. To investigate the seismic behavior of frames, nonlinear dynamic analysis was performed on these frames. Because, the SCB can provide a restoring force to buildings rather than a buckling-restrained brace (BRB), the earthquake response for these two brace frame systems may also be different. The object of this study was to formulate a loading protocol for first-story columns in dual system with SCBs during near-fault seismic events.

Eleven representative time histories of near-fault ground motion recorded in Taiwan were chosen to investigate the influence of SCBs on enhancing frame behavior. All of the selected records were characterized by ground motions featuring high acceleration, significant velocity pulses, and notable permanent displacement [5]. According to seismic design specifications and commentary of buildings (2011) [6] in

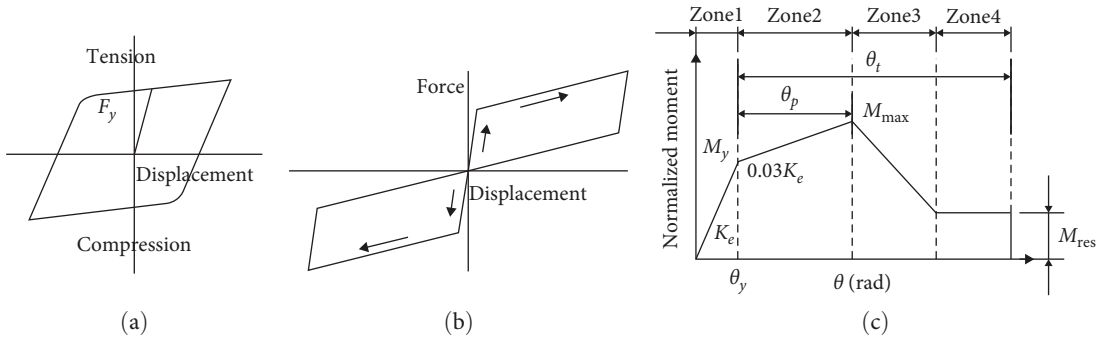

Figure 1: Hysteresis loop and backbone curve. (a) BRB; (b) SCB; (c) moment–rotation relation for steel members [7].

Taiwan, these earthquakes were scaled to meet the seismic intensity levels as the design basis earthquake (DBE) and maximum considered earthquake (MCE). Through nonlinear dynamic analysis, the seismic behaviors of four SCBFs were examined, and the dynamic response of the columns, beams, and SCBs were also obtained. Based on the analysis results, a loading protocol was formulated and proposed for the first-story column test, specifically for the lateral drift and axial force variation in SCBFs under near-fault earthquakes.

2. Literature Review

BRBs can yield and dissipate energy under tension and compression, and provide stability against buckling under compressive loads (Figure 1(a)). The hysteresis response of BRBs can considerably improve the seismic performance of a structure. However, BRBs can also cause residual deformation of structures, which becomes a critical problem in seismic design [8]. By contrast, the self-centering ability of SCBs (Figure 1(b)) can effectively reduce the lateral residual deformation of structures during earthquakes. A novel brace with self-centering energy-dissipative features was developed by Christopoulos et al. [2], which can significantly reduce the risk of structural damage, residual deformation, or collapse for structures under earthquakes. Chou and Chen [9] proposed a steel dual-core SCB that retains the advantages of traditional SCBs but has twice the axial elongation capacity. By performing cyclic tests with similar axial capacities on large-scale BRBs and SCBs, Chou et al. [10] found that the energy dissipation capacity of BRBs is considerably higher than that of SCBs, but SCBs have considerably smaller residual deformations because the posttensioning force provides restoring force in the SCBs. Chou et al. [11] further reported that SCBFs have higher energy dissipation than do BRBFs because the higher post-yield stiffness of SCBs can help the frame system to develop a higher strength, which can increase the energy dissipation of the frame as not see in a single SCB test. In addition to posttensioned SCBs, a brace using shape memory alloy (SMA) also exhibits a self-centering hysteretic response. Zhang and Zhu [12] demonstrated that prestrained SMA-based SCBs can efficiently reduce the drift ratio and floor acceleration of frames compared to unprestrained ones. Shi et al. [13] found that a higher initial stiffness of SMA-based SCBs results in a greater reduction of the residual drift and an improvement in collapse resistance during a large seismic event. Casagrande et al. [14] found that the SMA mechanic properties are affected by the temperature change. Ferraioli et al. [15] demonstrated the effectiveness of SMA-based SCBs installed in RC buildings on decreasing story drift and structural damage. Furthermore, they found that the recentering ability of the brace allows columns to be repairable after a large seismic event. Numerous studies have analyzed and compared the performance of MRFs, BRBFs, and SCBFs during earthquakes, but studies that specifically investigate the influence of near-fault earthquakes on these structures are insufficient. Tremblay et al. [16] showed that SCBFs can effectively reduce residual story drift under near-fault and far-field earthquakes, however, certain aspects of the behavior of SCBFs under near-fault earthquakes are still unclear.

Baker [17] revealed that near-fault motions increase the elastic seismic demand of structures with similar periods. Mohammadi et al. [18] studied the response of structures under near-fault earthquakes and reported that the velocity pulse would lead to ineffectiveness of the structural ductility and damage of structure. Gillie et al. [19] indicated that near-fault earthquakes increase the inelastic seismic demand of structures. Moniri [20] and Chou et al. [21] reported that buildings under near-fault motions exhibit larger deformation than do those under far-field motions. Furthermore, they reported that taller buildings tended to have stronger dynamic responses. Fang et al. [22] evaluated the response of different buildings under near-fault and far-field earthquakes. Building models of MRF, BRBF, and SCBF structures were constructed to conduct nonlinear dynamic analysis, and the results indicated that the deformation demands recommended by current design codes at the DBE and MCE levels were underestimates for near-fault earthquakes.

Researches have indicated that near-fault earthquakes and far-field earthquakes have distinct seismic characteristics that result in different effects on buildings. In current seismic design practices, near-fault effects are considered by using near-fault coefficients to modify the design spectra and increase the seismic design force. However, according to Krawinkler et al. [23], the near-fault coefficients may not accurately represent the properties of near-fault earthquakes and capture their impact on building drift demand. The current study was aimed to examine the response of SCBFs

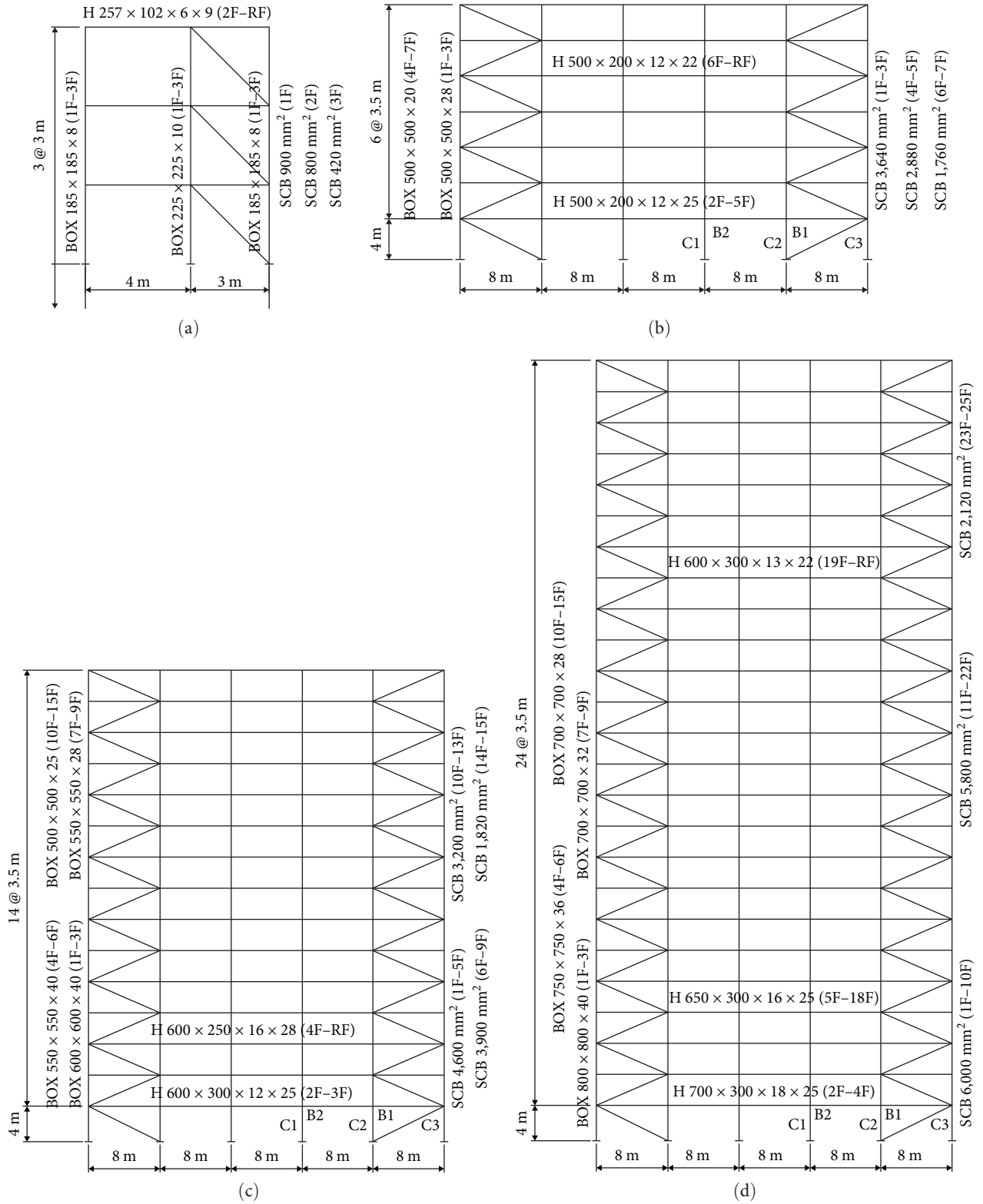

Figure 2: Continued.

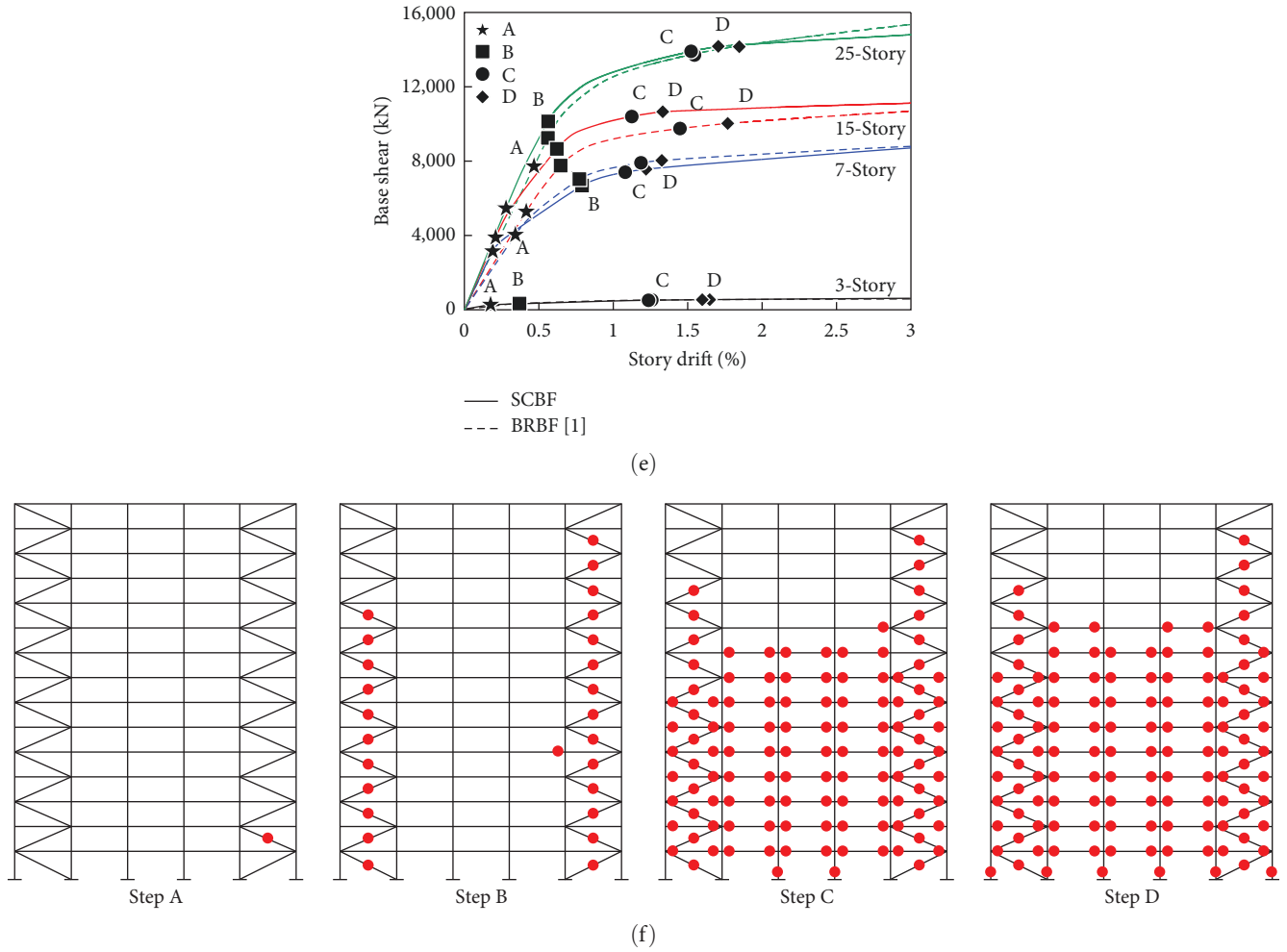

Figure 2: Dual systems with SCBFs and comparison of the pushover analysis results. (a) 3-Story, $T_1 = 0.36$ s; (b) 7-story, $T_1 = 0.83$ s; (c) 15-story, $T_1 = 1.56$ s; (d) 25-story, $T_1 = 2.47$ s; (e) pushover analysis results; (f) yielding order of 15-story.

in a series of near-fault earthquakes, with a focus on capturing the effects of such earthquakes on the first-story column. The lateral displacement and axial force variation of columns under near-fault earthquakes are uncertain, and a loading protocol for testing first-story columns in SCBFs has not been developed. Therefore, 3-, 7-, 15-, and 25-story buildings with steel dual-system frames comprising SMFs and SCBFs were investigated to evaluate the seismic behavior of the system as well as the first-story column response.

3. Steel Dual Systems with SCBs

3.1. Four Frames. As displayed in Figure 2, steel dual-system building models with 3, 7, 15, and 25 stories were established for seismic analysis. These models are presumed to be located near the Xinhua fault, at a distance of 3.5 km. The site is categorized as Class 2 with an average shear wave velocity of the soil layer ranging between 180 and 270 m/s. The design base shear and member dimensions of SCBFs and BRBFs are shown in Table 1. The design details of BRBFs can be found in Liu et al. [1]. The mode shapes and the fundamental periods of SCBFs are shown in Figure 3. For both BRBFs and SCBFs, the design seismic loads were determined according to the equivalent static force procedure of seismic design specifications and commentary of buildings (2011) [6] in Taiwan. A response modification coefficient R of 4.9 and an overstrength factor Ω_0 of 1.4 that are not the same as those in ASCE 7-16 [25] were used for BRBFs. A deflection amplification factor C_d of 5 was used for BRBFs because all beam–column connections were designed for the moment-resisting connections based on AISC 341 seismic provisions (2016). The same design values were considered for SCBFs to allow for a direct comparison. For SCBFs, the columns are constructed with box sections, while the beams are made of I-section. All members were made of SN490B steel ($F_y = 325$ MPa). The width-to-thickness (b/t) ratios of the columns in each frame (Table 2) meet the most compact requirement ($\lambda_{pd} = 24.77$) in design and technique specifications of steel structures for buildings (2007) in Taiwan [24], but the values are between those of the highly ductile ($\lambda_{hd} = 15.37$) and moderately ductile ($\lambda_{md} = 27.91$) limits in AISC 341-16 [4]. Recently, the width-to-thickness requirement for highly ductile steel built-up box columns is more stringent in AISC 341-22 [26] than in AISC 341-16 [4] or design and technique specifications of steel structures for buildings (2007) in Taiwan [24]. The moderately ductile steel box column cannot be used in the BRBF

Table 1: Base shear and element dimensions.

		Floor	SCBF	BRBF [1]
3-Story design base shear: 184 kN	Col.	1F–3F	C1: BOX 185 × 185 × 8 C2: BOX 225 × 225 × 10 C3: BOX 185 ×185× 8	C1: BOX 185 × 185 × 8 C2: BOX 225 × 225 × 10 C3: BOX 185 × 185 × 8
	Beam	2F-RF	H 257 × 102 × 6 × 9	H 257 × 102 × 6 × 8
	Brace	1F	$A_c = 900\,\text{mm}^2$ ($P_y = 331\,\text{kN}$)	$A_c = 900\,\text{mm}^2$ ($P_y = 300\,\text{kN}$)
		2F	$A_c = 800\,\text{mm}^2$ ($P_y = 294\,\text{kN}$)	$A_c = 800\,\text{mm}^2$ ($P_y = 260\,\text{kN}$)
		3F	$A_c = 420\,\text{mm}^2$ ($P_y = 155\,\text{kN}$)	$A_c = 400\,\text{mm}^2$ ($P_y = 130\,\text{kN}$)
7-Story design base shear: 3,125 kN	Col.	1F–3F	BOX 500×500×28	BOX 500 × 500 × 28
		4F–7F	BOX 500 × 500 × 20	BOX 500 × 500 × 20
	Beam	2F–5F	H 500 × 200 × 12 × 25	H 500 × 200 × 12 × 22
		6F-RF	H 500 × 200 × 12 × 22	H 500 × 200 × 12 × 20
	Brace	1F–3F	$A_c = 3{,}640\,\text{mm}^2$ ($P_y = 1{,}338\,\text{kN}$)	$A_c = 3{,}640\,\text{mm}^2$ ($P_y = 1{,}200\,\text{kN}$)
		4F–5F	$A_c = 2{,}880\,\text{mm}^2$ ($P_y = 1{,}059\,\text{kN}$)	$A_c = 2{,}880\,\text{mm}^2$ ($P_y = 950\,\text{kN}$)
		6F–7F	$A_c = 1{,}760\,\text{mm}^2$ ($P_y = 647\,\text{kN}$)	$A_c = 1{,}760\,\text{mm}^2$ ($P_y = 580\,\text{kN}$)
15-Story design base shear: 3,814 kN	Col.	1F–3F	BOX 600 × 600 × 40	BOX 600 × 600 × 35
		4F–6F	BOX 550 × 550 × 40	BOX 550 × 550 × 32
		7F–9F	BOX 550 × 550 × 28	BOX 550 × 550 × 22
		10F–15F	BOX 500 × 500 × 25	BOX 500 × 500 × 22
	Beam	2F–3F	H 600 × 300 × 12 × 25	H 600 × 250 × 13 × 22
		4F–8F	H 600 × 250 × 16 × 28	H 600 × 250 × 12 × 20
		9F-RF	H 600 × 250 × 16 × 28	H 600 × 200 × 12 × 20
	Brace	1F–5F	$A_c = 4{,}600\,\text{mm}^2$ ($P_y = 1{,}693\,\text{kN}$)	$A_c = 4{,}550\,\text{mm}^2$ ($P_y = 1{,}500\,\text{kN}$)
		6F–9F	$A_c = 3{,}900\,\text{mm}^2$ ($P_y = 1{,}435\,\text{kN}$)	$A_c = 3{,}940\,\text{mm}^2$ ($P_y = 1{,}300\,\text{kN}$)
		10F–13F	$A_c = 3{,}200\,\text{mm}^2$ ($P_y = 1{,}178\,\text{kN}$)	$A_c = 3{,}030\,\text{mm}^2$ ($P_y = 1{,}000\,\text{kN}$)
		14F–15F	$A_c = 1{,}820\,\text{mm}^2$ ($P_y = 670\,\text{kN}$)	$A_c = 1{,}820\,\text{mm}^2$ ($P_y = 600\,\text{kN}$)
25-Story design base shear: 5,379 kN	Col.	1F–3F	BOX 800 × 800 × 40	BOX 800 × 800 × 36
		4F–6F	BOX 750 × 750 × 36	BOX 750 × 750 × 36
		7F–9F	BOX 700 × 700 × 32	BOX 700 × 700 × 32
		10F–25F	BOX 700 × 700 × 28	BOX 700 × 700 × 28
	Beam	2F–4F	H 700 × 300 × 18 × 25	H 650 × 300 × 18 × 25
		5F–18F	H 650 × 300 × 16 × 25	H 650 × 300 × 15 × 25
		19F-RF	H 600 × 300 × 13 × 22	H 600 × 300 × 13 × 22
	Brace	1F–3F	$A_c = 6{,}000\,\text{mm}^2$ ($P_y = 2{,}208\,\text{kN}$)	$A_c = 6{,}060\,\text{mm}^2$ ($P_y = 2{,}000\,\text{kN}$)
		4F–10F	$A_c = 6{,}000\,\text{mm}^2$ ($P_y = 2{,}208\,\text{kN}$)	$A_c = 5{,}430\,\text{mm}^2$ ($P_y = 1{,}800\,\text{kN}$)
		11F–19F	$A_c = 5{,}800\,\text{mm}^2$ ($P_y = 2{,}134\,\text{kN}$)	$A_c = 4{,}550\,\text{mm}^2$ ($P_y = 1{,}500\,\text{kN}$)
		20F–22F	$A_c = 5{,}800\,\text{mm}^2$ ($P_y = 2{,}134\,\text{kN}$)	$A_c = 3{,}030\,\text{mm}^2$ ($P_y = 1{,}000\,\text{kN}$)
		23F–25F	$A_c = 2{,}120\,\text{mm}^2$ ($P_y = 780\,\text{kN}$)	$A_c = 2{,}120\,\text{mm}^2$ ($P_y = 700\,\text{kN}$)

	3-Story	7-Story	15-Story	25-Story
SCBF	0.36	0.83	1.56	2.47
BRBF	0.44	1.01	1.94	2.77

Note: first mode periods (s)

according to AISC 341-22 [26], which requires a much thicker steel plate for column design in a high-seismic area, same design concept used for the new braced frame system-SCBF in this work. To investigate if the design requirement is suitable for steel built-up box columns, this study was focused on earthquake demands on first-story steel box columns in SCBFs, such as lateral drift and axial loading histories.

For the 3-story model, the design static load (DL) is 18.13 kPa and the design live load (LL) is 5.15 kPa. For the 7-, 15-, and 25-story models, the design DL is 8.8 kPa, and the design LL is 2.9 kPa. The first-story column axial forces are defined as follows: $P_g = 1.0DL + 0.5LL$, $P'_g = 1.2DL + 1.6LL$, and $P_u = 1.2DL + 0.5LL \pm 1.0E + 0.3E_v$, where E stands for the horizontal seismic force and E_v represents vertical seismic force. The capacity-to-demand ratio (DCR) of columns is computed using $\text{DCR} = \frac{P_r}{P_C} + \frac{8}{9}\frac{M_r}{M_C} < 1.0$ when $\frac{P_r}{P_C} \geq 0.2$, and $\text{DCR} = \frac{P_r}{2P_C} + \frac{M_r}{M_C} < 1.0$ when $\frac{P_r}{P_C} < 0.2$. The parameters P_r and P_c are the axial forces caused by loads and earthquake forces and expected axial strength, respectively;

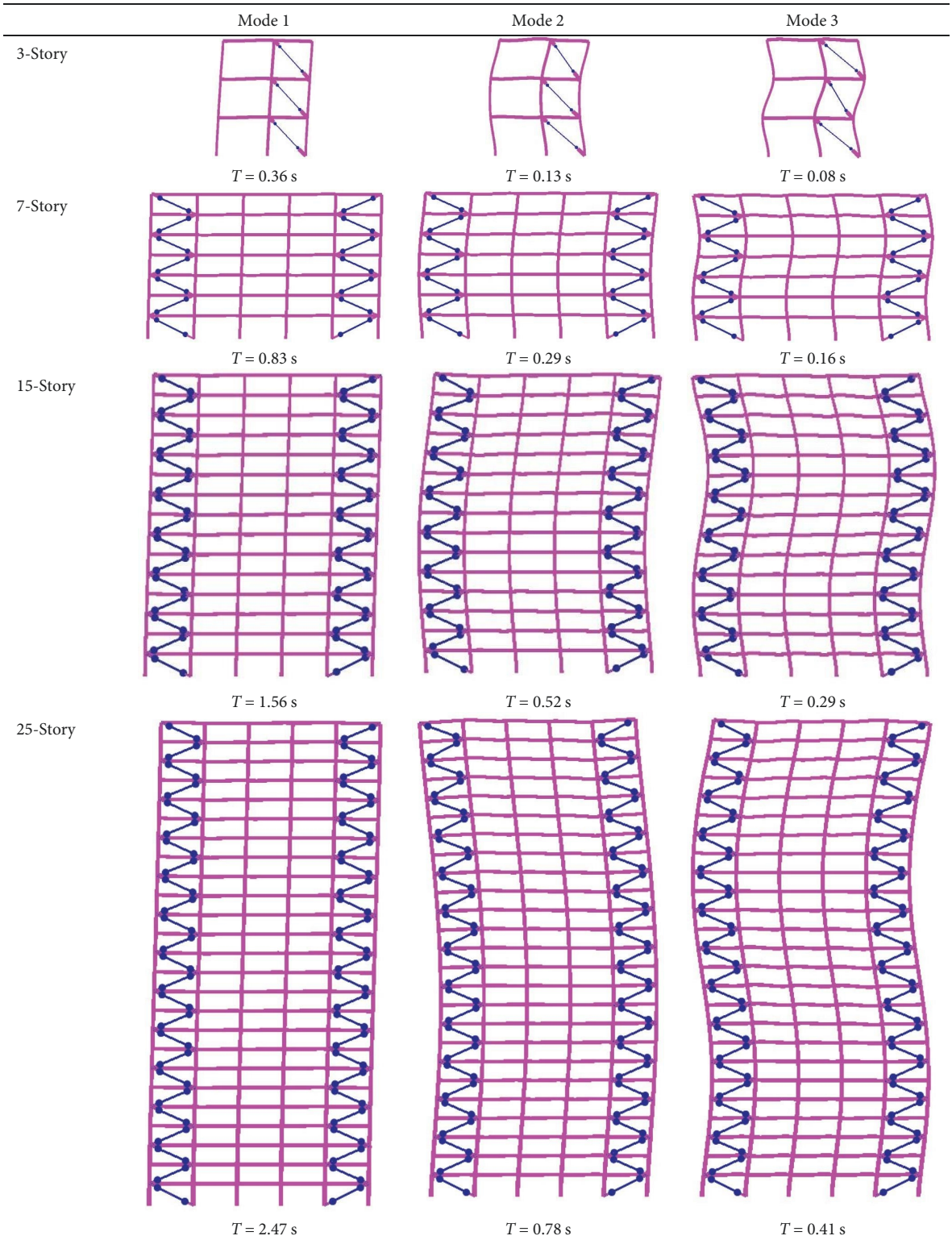

Figure 3: The first three mode shapes for the SCBF.

M_r refers to the required strength of moment, whereas M_c is the moment capacity. The DCR values are all below 1.0 as cataloged in Table 2, which indicate that the columns on the first story have been designed to satisfy the seismic demand.

3.2. Element Modeling. Nonlinear analyses of the braced frames were performed using the PISA3D program [27]. The beams and columns were simulated as bilinear while the ratio of post-elastic stiffness to the elastic stiffness was 3%. Backbone curve parameters of the columns and beams

Table 2: Axial force ratio of the first-story columns.

	First-story column	A (cm^2)	b/t	$P_y = R_y F_y A$ (kN)	$C_g = P_g/P_y$	$C_{g'} = P_{g'}/P_y$	$C_a = P_u/P_y$	DCR
3-Story	C1: BOX 185 × 185 × 8	57	21.1	2025	0.12	0.17	0.15	0.55
	C2: BOX 225 × 225 × 10	86	20.5	3,075	0.15	0.21	0.30	0.61
	C3: BOX 185 × 185 × 8	57	21.1	2025	0.08	0.12	0.21	0.54
7-Story	C1: BOX 500 × 500 × 28	529	15.9	18,899	0.25	0.37	0.31	0.65
	C2: BOX 500 × 500 × 28	529	15.9	18,899	0.23	0.34	0.39	0.76
	C3: BOX 500 × 500 × 28	529	15.9	18,899	0.14	0.20	0.31	0.68
15-Story	C1: BOX 600 × 600 × 40	896	13	28,713	0.34	0.50	0.43	0.72
	C2: BOX 600 × 600 × 40	896	13	28,713	0.30	0.44	0.49	0.80
	C3: BOX 600 × 600 × 40	896	13	28,713	0.22	0.33	0.48	0.78
25-Story	C1: BOX 800 × 800 × 40	1,216	18	43,472	0.36	0.54	0.46	0.82
	C2: BOX 800 × 800 × 40	1,216	18	43,472	0.32	0.47	0.51	0.88
	C3: BOX 800 × 800 × 40	1,216	18	43,472	0.26	0.39	0.60	1.00

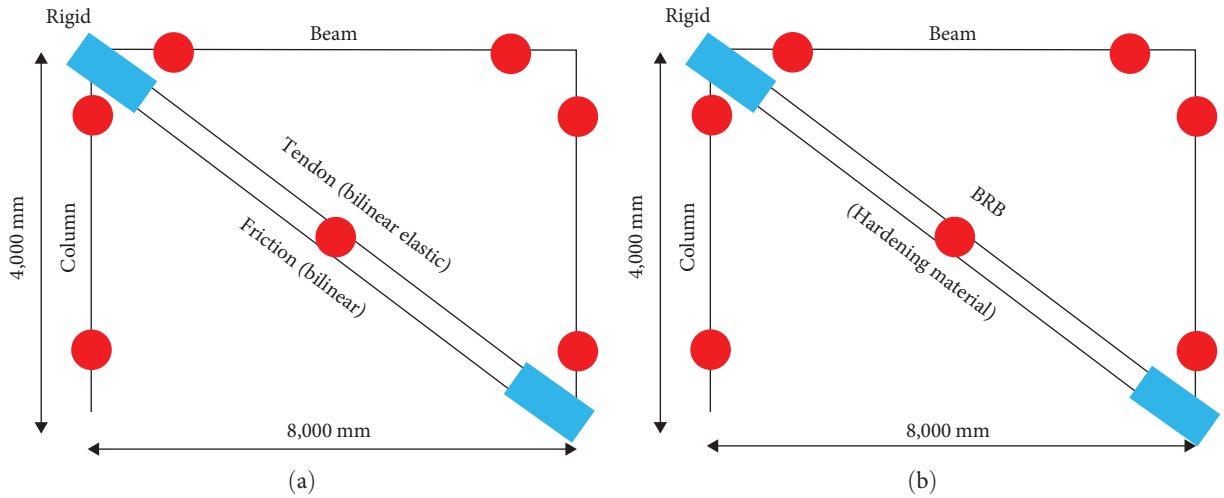

Figure 4: SCBF and BRBF simulation. (a) SCBF and (b) BRBF.

were derived from ASCE 41-17 [7], which took into account the axial force in the column for the M_y and the yield rotation. A 3% damping ratio for all frames was assigned for steel structures. Additionally, the P-Delta effect was taken into consideration as well. Since the structure system simulated in PISA3D still falls within the theoretical range of small deformation, the analysis considered the P-Delta effect by adding a simple geometric stiffness matrix and updating the matrix before each step, rather than updating the coordinates of the nodes [28, 29]. The rigid-zone factor was considered to simulate stiffness region at the end offset of structural members for the beam-to-column connections. In this study, it was set as 1 for the columns (fully rigid) and 0.75 for the beams. Figure 1(c) shows an example of the backbone curve parameters for columns conforming to ASCE 41-17 [7].

Truss elements were utilized to model the hysteretic response of the SCB as shown in Figure 4(a). The initial prestressing of the tension elements was assumed to be 52% of the axial brace force, which exceeded 48% of the force given by the friction of energy dispersion, so that the self-centering response of the brace can be maintained. The tension member and friction member were simulated by using bilinear-elastic and bilinear materials, and these two truss elements were connected in parallel. According to the study of Chou et al. [10], the elastic stiffness of the SCB could be assumed to be twice that of the corresponding BRB, and the ratio of the post-elastic stiffness relative to the elastic stiffness was set as 0.04 for the SCB. It was assumed that the SCB's length was 70% of the diagonal length of the frame, while the remaining portion was considered to be the gusset length (marked by a blue box at the brace ends in the Figures 4(a) and 4(b)). A truss element that combines both isotropic and kinematic hardening material properties was employed to model the hysteretic response of a BRB (Figure 5(b)), as outlined by Chou et al. [30]. The simulation results were correlated well with the experimental results of the SCB and BRB (Figures 5(a) and 5(b)).

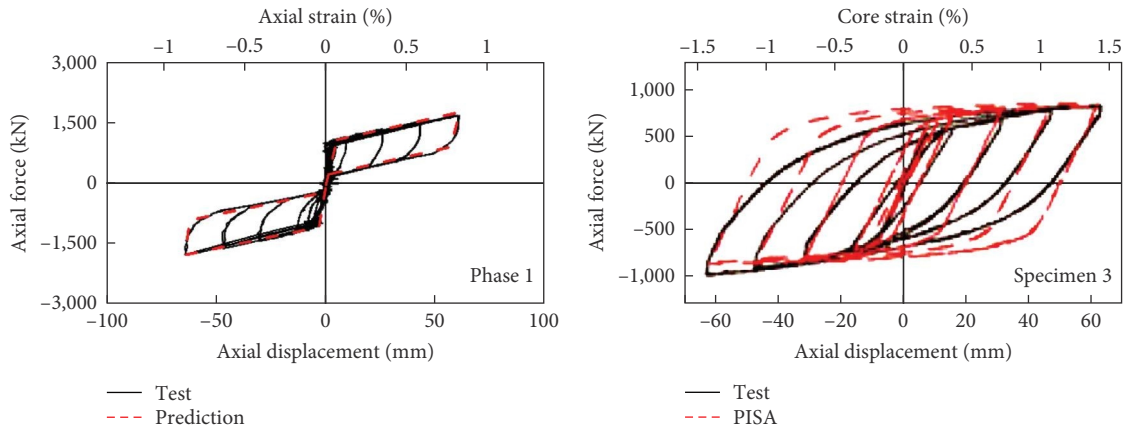

Figure 5: Comparison between the test and modeling of braces. (a) SCB [10] and (b) BRB [30].

Table 3: Eleven near-fault ground motions.

No.	Event	Station	Original PGV (cm/s)	Original PGA (g)	Scale factor (DBE)			
					3-Story	7-Story	15-Story	25-Story
NF1	ChiChi	CHY101EW	72.65	0.34	1.28	1.40	1.29	1.22
NF2	ChiChi	TCU029EW	35.16	0.16	2.49	2.71	2.68	2.78
NF3	ChiChi	TCU029NS	55.38	0.2	2.21	2.39	2.53	2.16
NF4	ChiChi	TCU031EW	53.72	0.11	3.54	3.78	3.34	2.94
NF5	Jiasian	CHY058EW	41.53	0.28	1.58	1.23	1.16	1.27
NF6	ChiChi	TCU054EW	41.75	0.15	2.29	2.28	2.15	2.30
NF7	ChiChi	TCU065EW	140.45	0.79	0.78	0.67	0.60	0.62
NF8	ChiChi	TCU053EW	41.9	0.23	1.19	1.30	1.78	1.22
NF9	ChiChi	TCU101EW	44.3	0.21	1.59	1.69	1.70	1.83
NF10	Hualian	HWA028NS	42.21	0.39	1.01	1.28	1.23	1.34
NF11	Hualian	HWA062NS	58.66	0.2	2.18	2.18	1.88	1.65

4. Nonlinear Static Procedure of Four SCBFs

Since the nonlinear pushover analysis is based on the assumption of an equivalent single-degree-of-freedom model, it may neglect the higher mode effect on the building response. Therefore, Chou and Uang [31] used the first two mode pushover analyses to estimate the inelastic energy distribution along the low-to-medium-rise building height without performing time history analyses of frames. To improve the accuracy and effectiveness of the displacement demand prediction for high-rise buildings, Poursha et al. [32] estimated the structural demand by enveloping the responses from multi- and single-stage analyses. Sucuoğlu and Günay [33] used a generalized force pattern that merged the modal forces to represent the force distribution along the structure induced by seismic events. Kreslin and Fajfar [34] extended the N2 method by assuming the vibration of structures in higher modes in the elastic state. Ferraioli et al. [35] used an actual displacement function to define an equivalent single-degree-of-freedom system at each incremental stage of the pushover analysis. Liu and Kuang [36] simplified the complex coupling between distinct modes and used the consecutive pushover technique to predict the structure demands. Ferraioli [37] demonstrated that the modal combination of the equivalent bilinear single-degree-of-freedom system effectively estimates the target drift of the multi-mode pushover analysis. Rahmani et al. [38] adopted the upper-bound pushover analysis by modifying a load pattern at each incremental stage to take into account the inelastic behavior of buildings. To examine the plastic hinge formation sequence in these frames, a nonlinear static pushover analysis with a displacement control was conducted on the four dual-system frame structures. Before performing the pushover analysis, the frame was subjected to the dead load and an additional 50% live load. Each frame was pushed using a lateral load distribution pattern in the shape of a reversed triangle. The lateral load pattern is similar to the first mode shape, not considering the high mode contribution in the static nonlinear pushover analysis because the high mode effect would be included in the nonlinear dynamic analysis of these frames in the next section. The beam and column elements utilize a concentrated hinge model to consider the nonlinear effects [29]. When the element remains in the

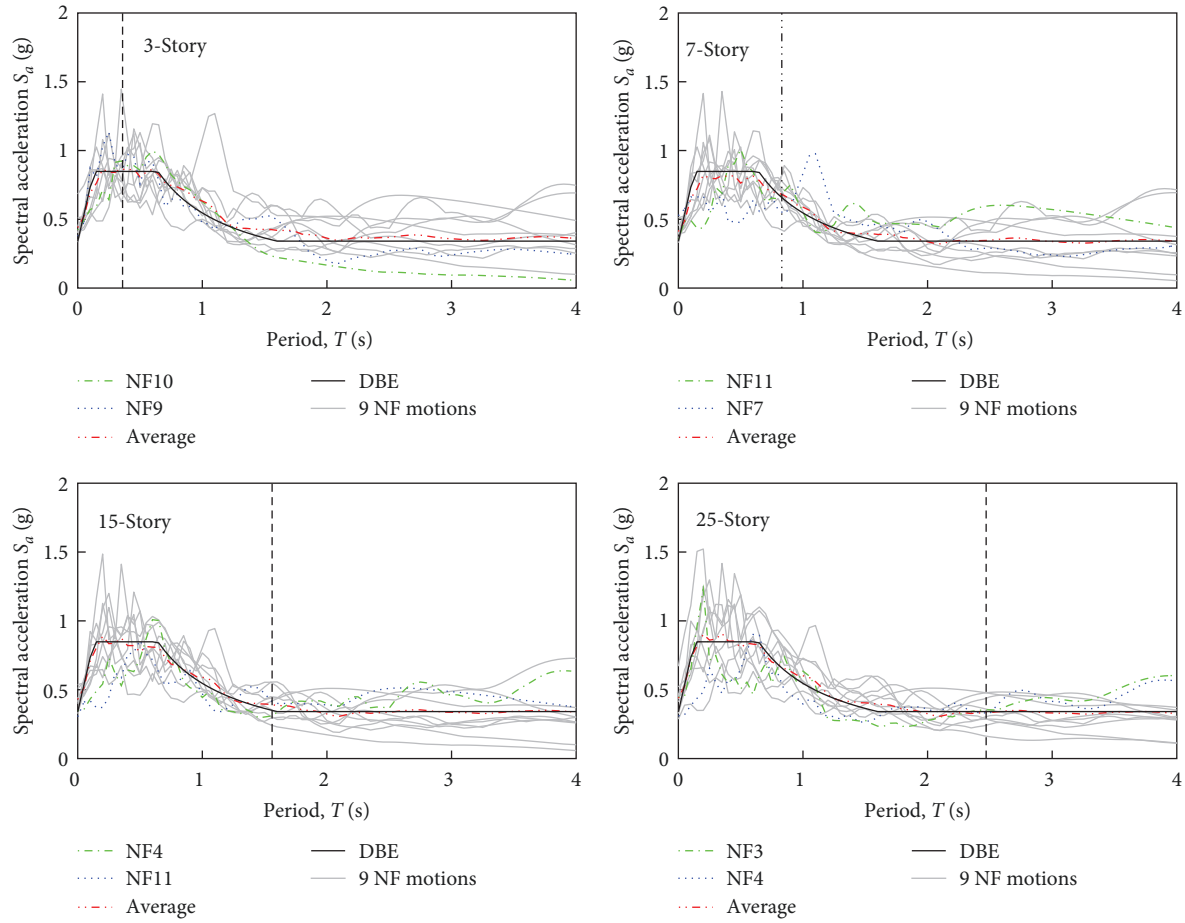

Figure 6: Response spectrum of the 11 near-fault earthquakes (DBE).

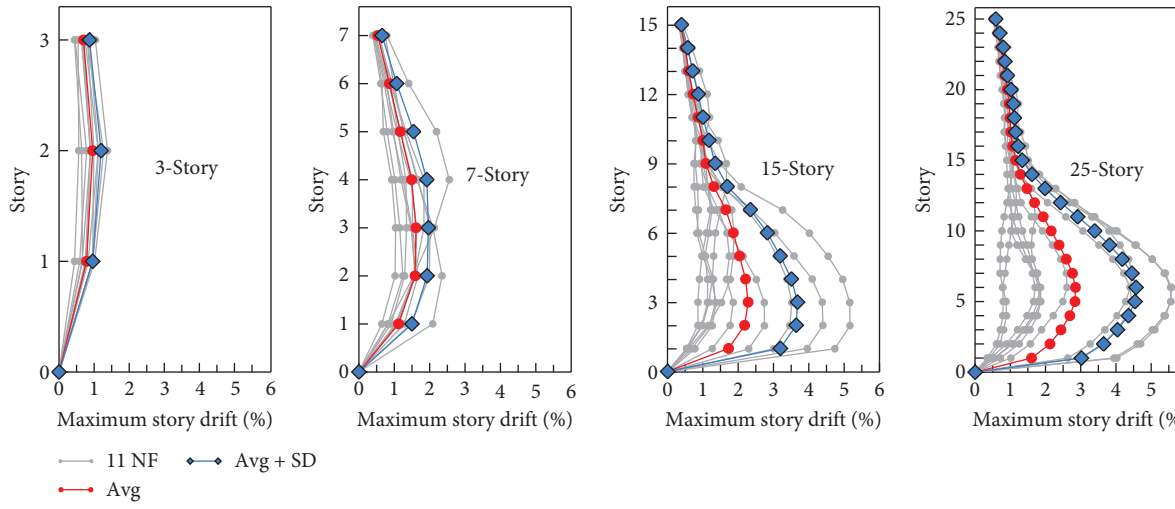

Figure 7: Maximum interstory drifts (MCE).

elastic range, the deformation occurs through the elastic element. Once the element is in a nonlinear state, the plastic deformation occurs through a plastic hinge at two ends of the element. Figure 2(e) shows the relationship between the base shear and the roof displacement; the first plastic hinge was formed after the design seismic force level (Table 1). Figure 2(e) also reveals that the SCBs started yielding (Step A) when the roof drift was in the range of 0.18%–0.28%, and the beams started to yield (Step B) at a roof drift between 0.32% and 0.8%. In all models, the initial plastic deformation

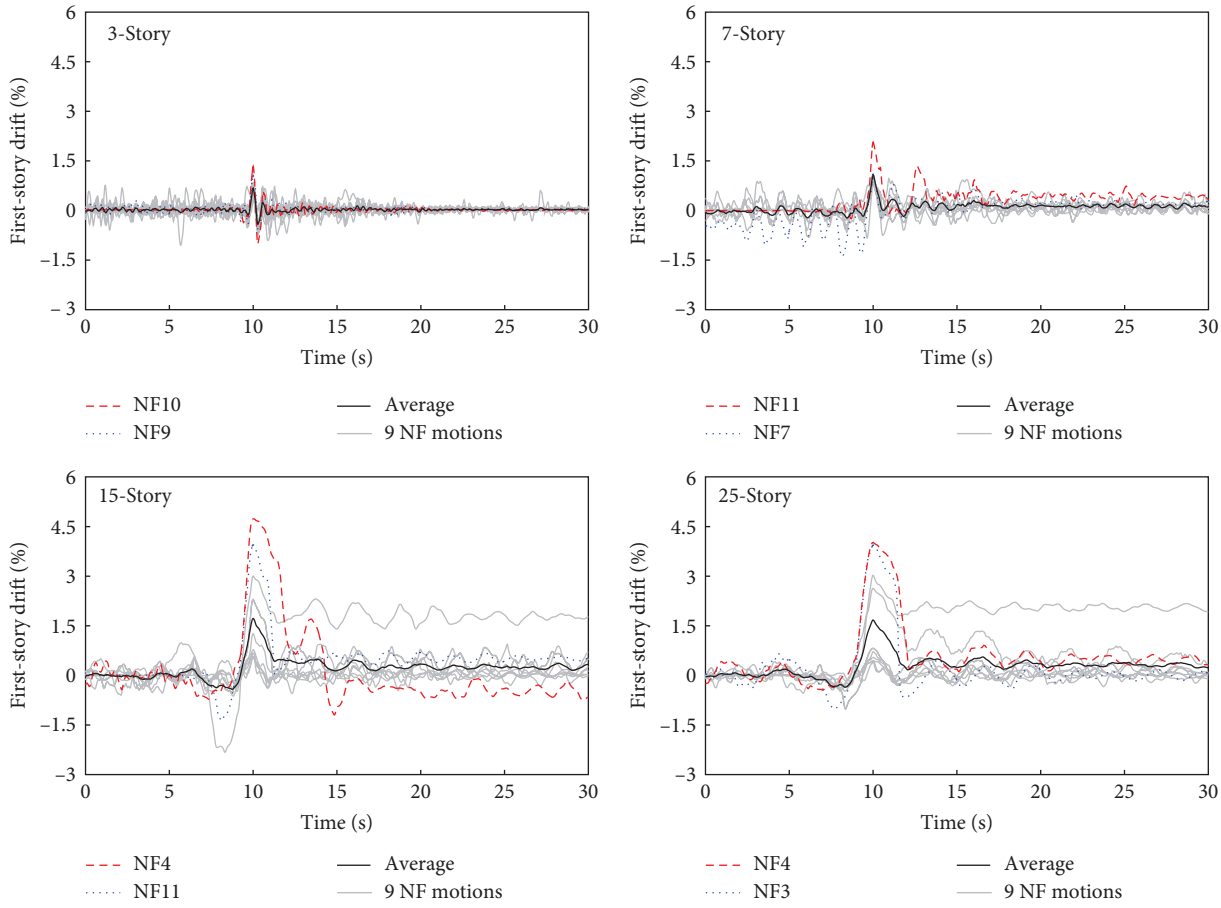

Figure 8: First-story drift histories (MCE).

at the base of the columns manifested (Step C), at the value of roof drift ranged from 1.08% to 1.52%, and every column on the ground floor yielded (Step D) when the value of roof drift varied within the range of 1.22%–1.71%. For example, Figure 2(f) showed the yielding sequence and the concentrated plastic hinge location of the 15-story SCBF. These results are consistent with the design principle of columns with higher strength relative to beams. A comparison of the results of nonlinear static pushover analysis for the SCBFs and the BRBFs reveals that the hinge formation sequence and the interstory drift are similar in both types of frames (Figure 2(e)).

5. Nonlinear Dynamic Procedures of Four SCBFs

To perform a nonlinear dynamic analysis, it is essential to use a minimum of 11 earthquakes according to ASCE 7-16 [25]. A total of 11 near-fault earthquakes were selected as the most significant seismic events and listed in Table 3, which were identified as a pulse-type ground motion as shown in Figure 6. These motions are denoted as Near-Fault 1 (NF1) to Near-Fault 11 (NF11). Following in ASCE 7-16 [25], the 11 time histories were modified in order to fulfill the design response spectrum prerequisites of the analyzed location, as shown in Figure 6. Table 3 catalogs scale factors for the 11 ground motions; which were adjusted on the basis using a minimum square error estimation [39]. Design response spectra and ground motions which are scaled to DBE level are shown in Figure 6. In the nonlinear dynamic analysis, all modified motions were multiplied by 1.5 for meet the MCE level. A vertical load of 1.0 DL + 0.5 LL was applied to all steel dual-system frames of the 3-, 7-, 15-, and 25-story buildings, and the frames were analyzed using the 11 time histories to obtain the seismic demands.

The mean highest interstory drift values of the four models with 3, 7, 15, and 25 stories are displayed in Figure 7. From the nonlinear dynamic analysis, the mean maximum first-story drifts were 0.7, 1.1%, 1.7%, and 1.6% for the corresponding models. The highest story drifts of all floors in the 3-, 7-, 15-, and 25-story frames were 1.0, 1.6%, 2.5%, and 2.9%, respectively. In addition, the seismic responses at higher floors tend to be smaller because of the dimensional continuity of different floor members. Typically, the columns, beams, and SCBs on upper levels have lower force demands compared to those on the lower levels. Figure 8 demonstrates that the highest first-story drift values (corresponding ground motions) of the 3-, 7-, 15-, and 25-story frames are 1.33 (NF10), 2.07 (NF11), 4.74 (NF4), and 4.02% (NF4), respectively. These large drifts occurred due to the presence of velocity pulses (Figure 9), especially in the cases of the NF4 and NF11 time histories. The maximum ground

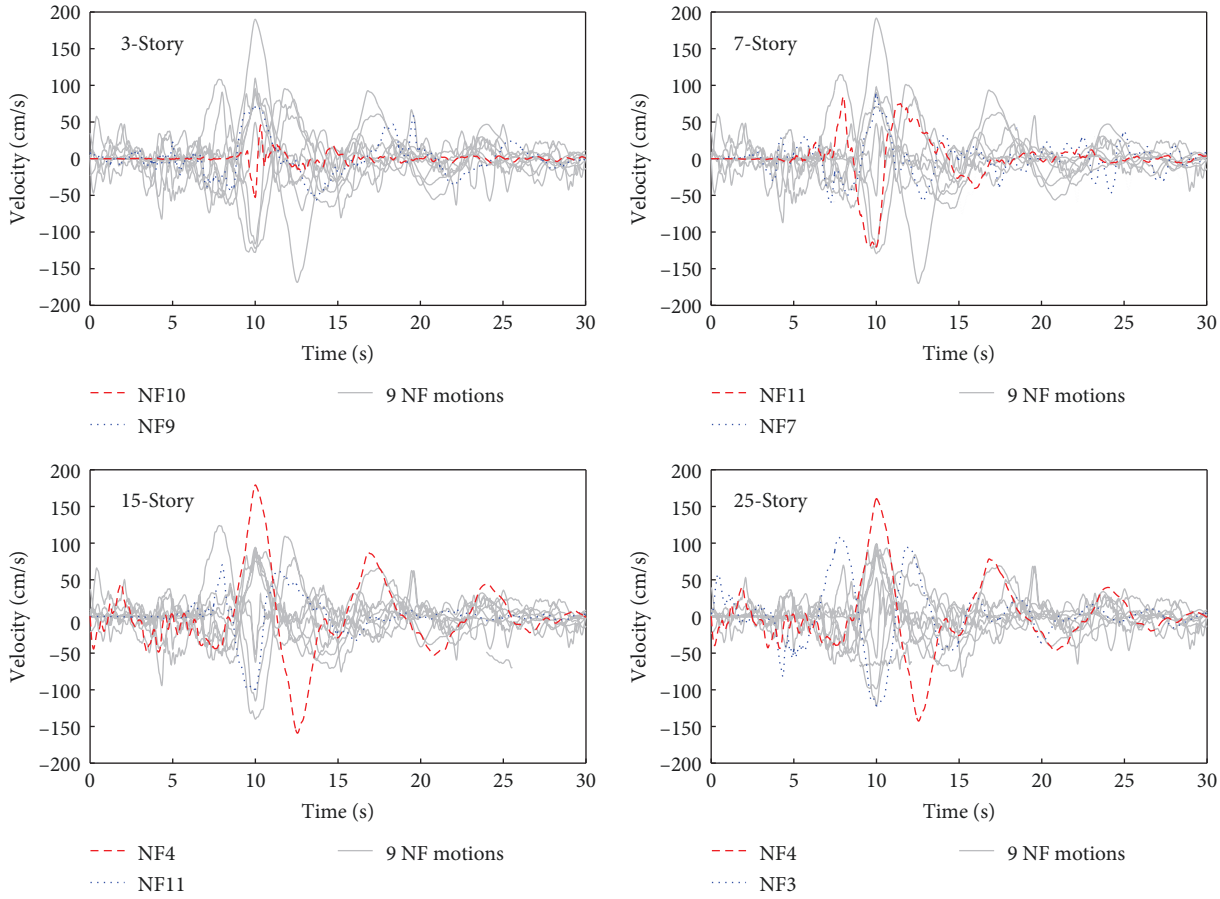

Figure 9: Velocity histories (DBE).

velocities of these motions were 53.7 and 58.7 cm/s, and the scale factors were 3.34 and 1.88, respectively (Table 3).

6. Loading Protocols of the Columns

The approach of Lin and Chou [39] was adopted for developing loading protocols of frames with SCBs, with an additional standard deviation incorporated to account for the variability in seismic parameters for different structures and earthquakes, as proposed by Fang et al. [40]. Figure 10(a) presents the displacement loading protocols of the four dual-system frames. Each protocol is calculated from the nonlinear dynamic analysis under 11 motions. Table 4 presents the count of displacement cycles associated with the 15-story frame under each time history analysis. Zone A represents the 10-s interval before the maximum story drift, Zone B covers the positive and negative maximum story drift, and Zone C encompasses the 20 s following the maximum story drift, including residual drift. The average drift cycles along with one standard deviation are shown in Figure 10(a). The loading protocols were used to capture the real seismic behavior of the columns on the first floor that experienced permanent residual drift during near-fault earthquakes. It is observed that the 3- and 7-story frames have smaller residual drifts compared to the 15- and 25-story buildings.

The exterior columns are connected to SCBs and may be subjected to larger forces than forces acting on the interior columns during earthquakes. Therefore, the outer first-story column C3 (Figure 2) was selected to evaluate an axial force loading procedure for SCBFs subjected to near-fault seismic motions. Figure 10(b) presents the proposed axial loading protocols of four frames and Table 5 provides the information on the numbers of cycles for the C3 column in the 15-story frame. The taller buildings have higher variations in axial load because of overturning and the connection of the C3 column to the SCBs. For example, the maximum axial force ratio for the 25-story frame is nearly $0.9P_y$. Figure 10(c) illustrates the correlation between the protocols of the axial force and the lateral displacement developed for the 15-story dual system. Upon impact of the earthquake pulse on the frame, the column on the first floor may deform to 3.5%, and the corresponding axial load is $0.56P_y$. This result can be used to determine the near-fault effect for the column test.

7. Response Comparison of Dual System with SCBFs and BRBFs

Compared with a dual system with BRBF [1], SCBFs have higher stiffness, which results in shorter structural periods with slightly larger member sizes (Table 1). A comparison of the nonlinear static analysis results for dual systems with

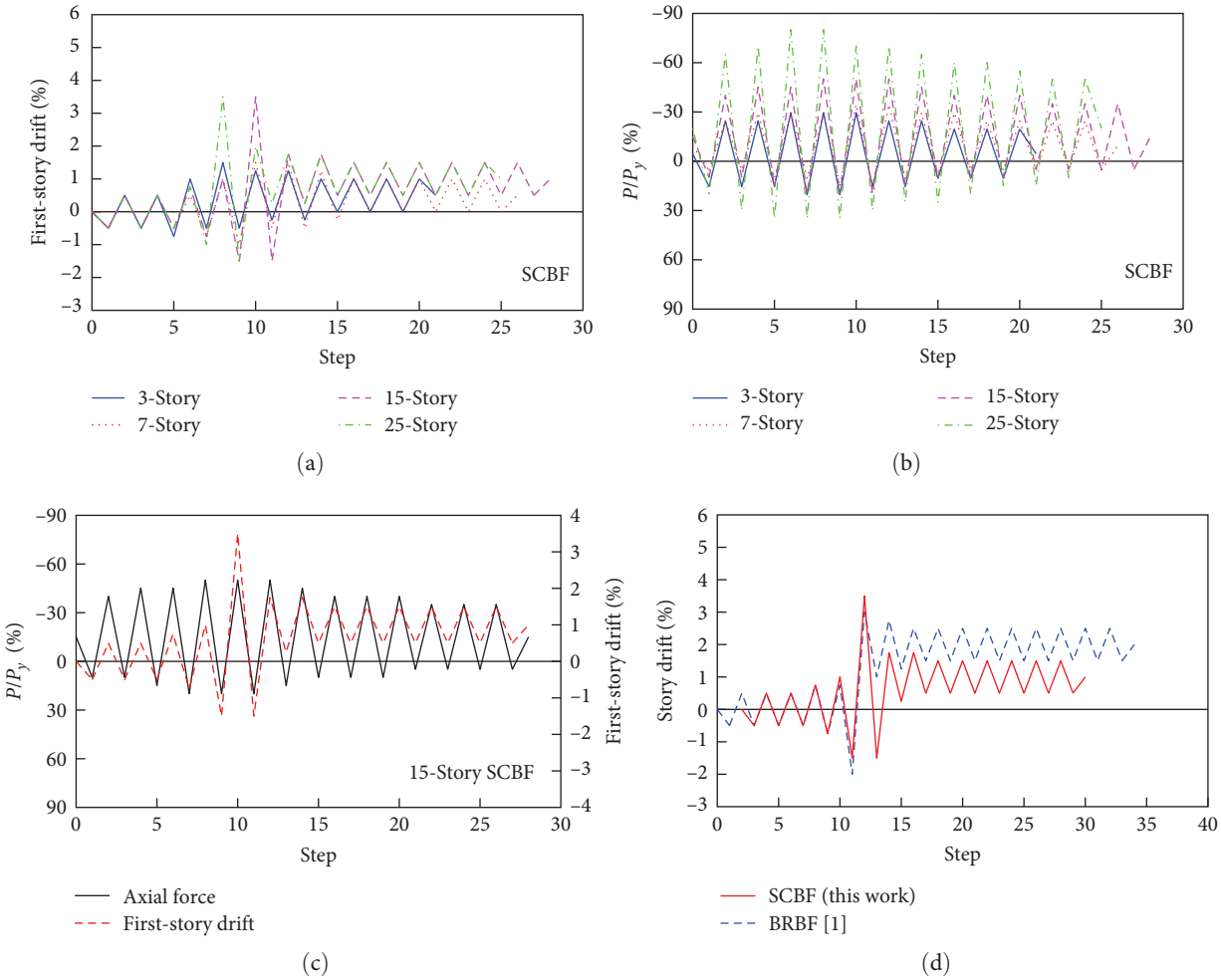

Figure 10: Proposed loading protocols of dual systems with SCBFs (Avg + SD). (a) Lateral drift; (b) axial force; (c) column C3; (d) comparison of dual system with SCBFs and BRBFs.

Table 4: Data of the lateral displacement loading protocols.

15-Story	First-story drift	NF1	NF2	NF3	NF4	NF5	NF6	NF7	NF8	NF9	NF10	NF11	Avg	SD	Avg + SD
Zone A	0.25%–0.5%	3.5	1.5	2	2	0	0.5	2	2	1	0	0	1.32	1.12	2.44
	0.5%–0.75%	0.5	0	1	2	0	0.5	0.5	0	0	0	0	0.41	0.63	1.03
	0.75%–1%	0	0	1	0	0	0	0	0	0	0	0	0.09	0.30	0.39
Zone C	0.25%–0.5%	7	2.5	5	2.5	3.5	6	8.5	1	1	1	2.5	3.68	2.59	6.27
	0.5%–0.75%	0.5	0.5	0	0	0.5	1	3	0.5	0.5	0	0.5	0.64	0.84	1.48
Zone B	Valley drift (%)	−0.52	−0.42	−2.33	−1.20	−0.47	−0.53	−0.63	−0.38	−0.48	−0.49	−1.37	−0.80	0.60	−1.40
	Peak drift (%)	2.30	0.78	3.01	4.74	0.60	0.55	1.26	0.68	0.57	0.54	3.95	1.72	1.54	3.26
	Residual drift (%)	0.47	0.11	1.83	0.45	0.02	0.00	0.39	0.05	0.02	0.00	0.65	0.36	0.54	0.90

SCBFs and BRBFs shows that the yielding sequence in steps A, B, C, and D, which represent yielding of SCB, beam, first column at first story and all first-story columns, respectively, are similar (Figure 2(e)). Therefore, dual systems with SCBFs and BRBFs have similar seismic performance. Figure 11(b)−11(d) show the average peak story drifts of the BRBF and SCBF, which exhibit similar drift patterns. For example, in the case of 15-story frames, the BRBF and SCBF exhibit the highest story drift at the third and fourth floors, in which the average maximum drift values are 2.77% and 2.25%, respectively (Figure 11(c)). The maximum story drift values for the SCBFs are also similar to those of the BRBFs (Figures 11(a) and 11(c)). However, the residual drift of the SCBFs is clearly lower than the BRBFs (Figure 12(a)−12(d)), which can be attributed to their self-centering capability (Figure 12(b)−12(d)). The residual drift in the first story of the 15-story SCBF under

Table 5: Data of the axial loading protocols (C3 column).

15-Story	P/P_y	NF1	NF2	NF3	NF4	NF5	NF6	NF7	NF8	NF9	NF10	NF11	Avg	SD	Avg + SD
Zone A	0%–5%	0.5	0	0.5	1	0.5	0	0	2	0.5	4	0.5	0.86	1.19	2.05
	5%–10%	0	0	0	0	0	0	0	0.5	2	0	1	0.32	0.64	0.96
	10%–15%	0	0	0	2	0.5	0.5	0	0	0	0	1	0.36	0.64	1.00
	15%–20%	0	1.5	0	0.5	1	0	1	0	1	0	0	0.45	0.57	1.02
	20%–25%	2.5	2.5	0	1	0	1	1	0	0.5	0	0	0.77	0.96	1.73
	25%–30%	2	0.5	1.5	0.5	0.5	2	2	0.5	0	0	0	0.86	0.84	1.70
	30%–35%	0	0	0.5	0	0	2.5	1	0	0	0	0	0.36	0.78	1.14
	35%–40%	0	0	0	0	0	0	0	0	0	0	0	0.00	0.00	0.00
	40%–45%	0	0	0	0	0	0	0	0	0	0	0	0.00	0.00	0.00
Zone C	0%–5%	1	1.5	1.5	1	0.5	0	0	1.5	0.5	0.5	1.5	0.86	0.60	1.46
	5%–10%	0.5	2.5	1.5	0	1.5	1.5	0	1.5	0	2	3.5	1.32	1.12	2.44
	10%–15%	1	3	2	2	2	2.5	0	1	2	3	2	1.86	0.90	2.76
	15%–20%	3.5	1.5	1.5	0.5	4	2.5	4	2.5	1.5	4	3.5	2.64	1.25	3.88
	20%–25%	1.5	1.5	2	2.5	2	3.5	5	0.5	0	0.5	0	1.73	1.54	3.27
	25%–30%	1.5	0	0	1	1	0	1.5	0	0	0	0	0.45	0.65	1.10
	30%–35%	0	0	0	0.5	0	0	0	0	0	0	0	0.05	0.15	0.20
	35%–40%	0	0	0	0	0	0	0	0	0	0	0	0.00	0.00	0.00
	40%–45%	0	0	0	0	0	0	0	0	0	0	0	0.00	0.00	0.00
Zone B	Peak (%)	−30.89	−26.56	−34.41	−34.64	−29.10	−28.57	−29.68	−34.29	−30.46	−27.39	−33.00	−30.82	2.89	−33.71
	Valley (%)	30.47	24.81	28.87	33.06	33.06	29.17	34.21	27.83	32.77	25.53	33.81	30.33	3.33	33.66

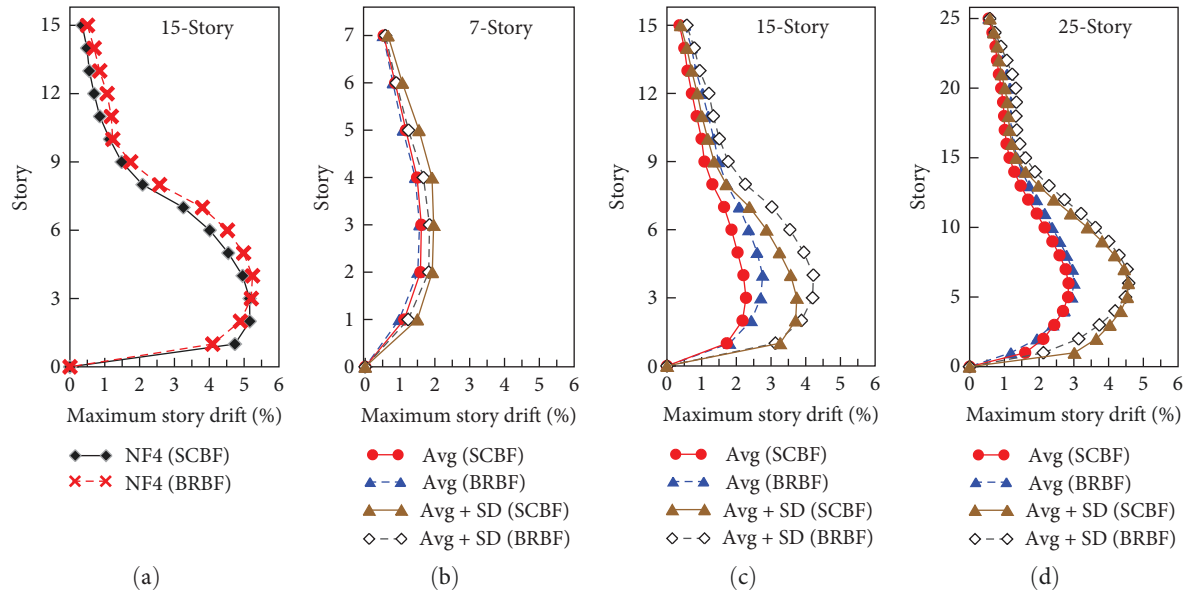

Figure 11: Comparison of the maximum story drift of dual systems with BRBFs and SCBFs (MCE). (a) 15-Story under the NF4; (b) 7-story (Avg/Avg + SD); (c) 15-story (Avg/Avg + SD); (d) 25-story (Avg/Avg + SD).

NF4 is less than 0.5%, whereas that of the BRBF is 2%. The residual drifts of all floors of the 15-story SCBF under NF4 are less than 0.5%, and the residual drifts of the BRBF below the 10th floor are higher than 0.5% (Figure 12(a)).

Moreover, according to the lateral displacement loading protocol of Liu et al. [1], the permanent residual drifts of the BRBF are approximately 1% and 2% (average and average + standard deviation); the corresponding values for the SCBF are approximately 0.5% and 1% (Figure 10(d) and Table 4). The member responses of two 15-story dual systems with SCBFs and BRBFs under the NF4 motion are plotted in Figure 13. The columns (Figure 13(a)–13(d)), beam B1 (Figure 13(e)), and brace (Figure 13(f)) are modeled in accordance with the element modeling method outlined in Section 3.2 and the hysteresis loops displayed in Figures 1(a) and 1(b). Column C2 is an interior column that

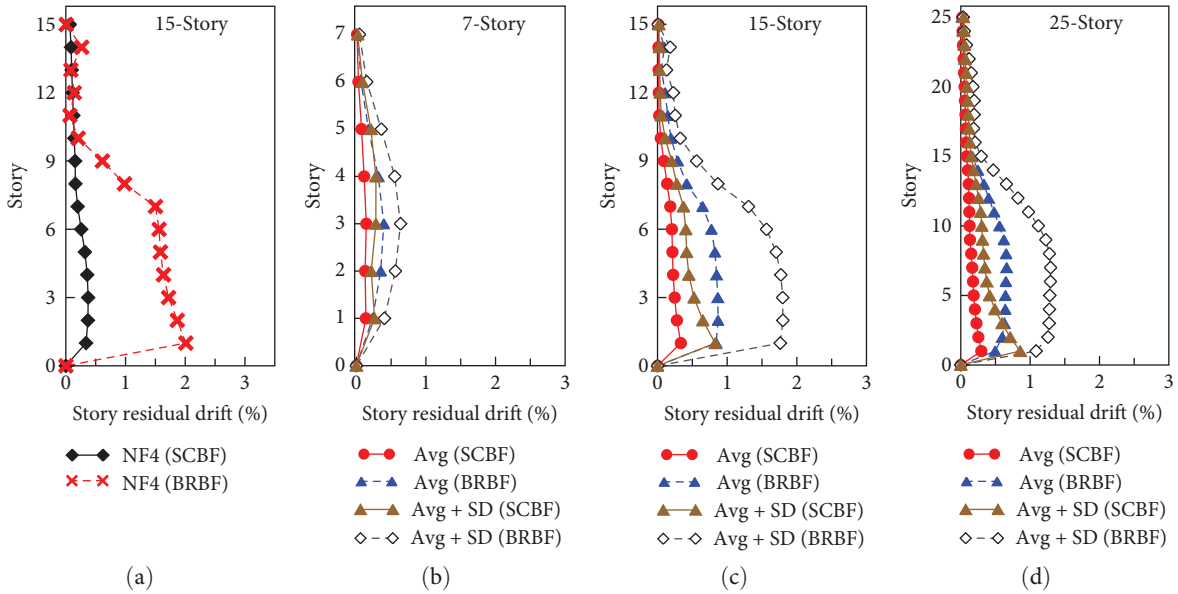

Figure 12: Comparison of the residual drift of dual systems with BRBFs and SCBFs (MCE). (a) 15-Story under the NF4; (b) 7-story (Avg/Avg + SD); (c) 15-story (Avg/Avg + SD); (d) 25-story (Avg/Avg + SD).

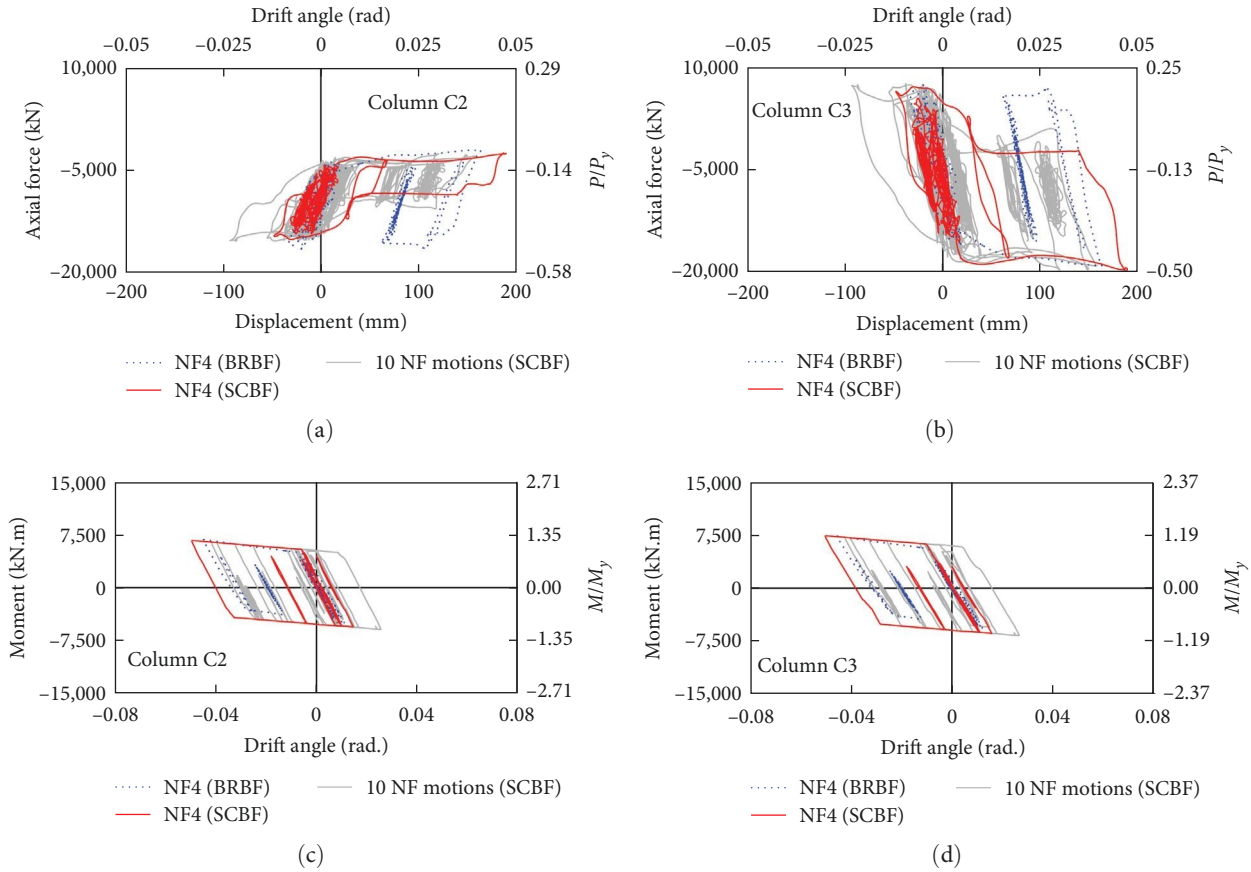

Figure 13: Continued.

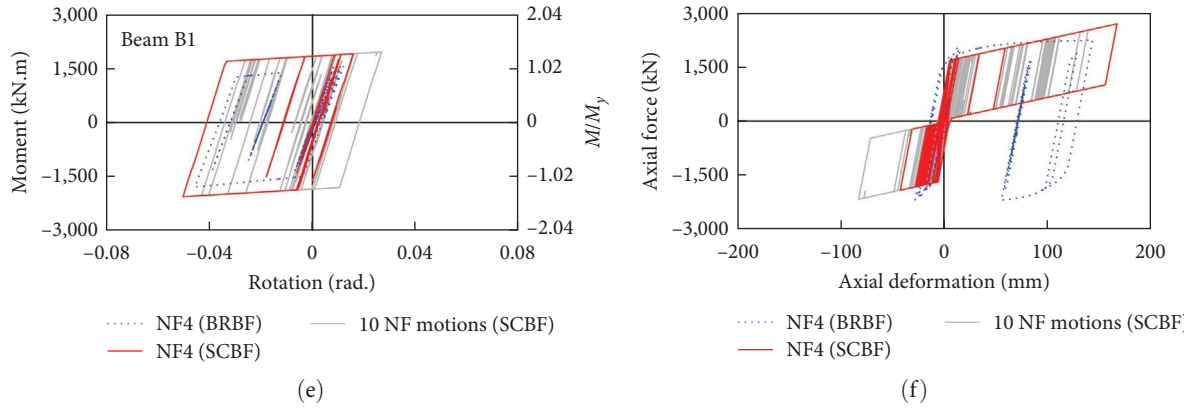

FIGURE 13: Comparison of the force-deformation relation for elements on the first-story of 15-story dual systems with BRBFs and SCBFs (MCE). (a) Axial force versus story drift of column C2; (b) axial force versus story drift of column C3; (c) moment versus story rotation of column C2; (d) moment versus story rotation of column C3; (e) moment versus rotation of beam, B1; (f) axial force versus deformation of SCB and BRB.

carries a higher DL and LL than does C3. The term P_y is normalized to the column yield axial force of the SCBFs. The exterior column is connected to SCBs, which results in the concentration of stiffness and makes it experience higher seismic forces compared to the interior columns (Figures 13(a) and 13(b)). Figure 13(f), for two different braces on the first floor, the SCB provides greater recentering capability compared to the BRB. Additionally, the SCB allows for a significant reduction in residual drift of the column, as shown in Figure 13(a)−13(d).

8. Conclusions

The object of this research was to establish axial force and lateral displacement protocols for columns on the first floor in a dual system with SCBFs exposed to near-fault seismic events. As shown in Table 1, the fundamental natural periods of the 3-, 7-, 15-, and 25-story SCBFs were 0.36, 0.83, 1.56, and 2.47 s, respectively. A total of 11 motions were selected for analysis in this study (Table 3), representing near-fault earthquakes with features of both considerable velocity pulses as well as significant peak ground accelerations.

Maximum story drifts and residual drifts of four dual systems with SCBFs under the 11 selected near-fault earthquakes were extracted and analyzed. To capture the most significant dynamic response of the frames, the 15-story building response was chosen to represent the loading protocol, developed for a conservative reason. With a maximum story drift of 3.5% and a residual drift of nearly 1% (in terms of average + standard deviation response), this loading protocol represents the response of first-story columns and a residual drift. The low-rise and mid-rise buildings have smaller residual drifts than the high-rise buildings. To compare with the lateral displacement protocol, the axial loading protocol was derived from for the outer column (C3) in the 15-story building, and the axial force ranged from 0.22 to 0.56 P_y.

Compared with a dual system with BRBFs, a dual system with SCBFs has similar maximum first-story drift but considerably lower residual drift (Figure 10(d)), which indicates that the SCB can considerably reduce residual deformation of frames. Therefore, SCBFs not only retain the high-seismic performance of BRBFs but also significantly reduce the residual drifts. Note that, residual drift exceeding the acceptable level of 0.5% for safety stated in FEMA P-1050-1 [41] may impact a building's functionality and require extensive retrofitting. As shown in Figure 12, no retrofitting is required for any floor of the short-, mid-, and long-period dual systems with SCBFs after the MCE earthquakes. However, substantial repairs are required for most dual systems with BRBFs. Since the permanent residual drift that of dual systems with SCBFs is notably lower than those with BRBFs, the use of SCBFs instead of BRBFs might considerably reduce repair and retrofitting costs after the occurrence of large near-fault earthquakes.

Data Availability

The data used to support the findings of this study are included within the manuscript.

Conflicts of Interest

The authors declare that they have no known competing financial interests or personal relationships that could have appeared to influence the work reported in this paper.

Acknowledgments

We would like to express our gratitude to the Central Meteorological Administration for providing earthquake data and to Dr. Zhao of the National Center for Research on Earthquake Engineering for selecting the most suitable time histories of ground motion. This research was supported by a grant from the National Science and Technology Council of Taiwan (Nos. 109-2625-M-492-010 and 110-2625-M-492-005).

References

[1] Y.-F. Liu, C.-C. Chou, G. R. Peng, and K.-J. Chen, "Development of near-fault loading protocols for first-story steel columns in dual systems with BRBs," *Journal of the Chinese Institute of Engineers*, vol. 46, no. 1, pp. 39–52, 2023.

[2] C. Christopoulos, R. Tremblay, H.-J. Kim, and M. Lacerte, "Self-centering energy dissipative bracing system for the seismic resistance of structures: development and validation," *Journal of Structural Engineering*, vol. 134, no. 1, pp. 96–107, 2008.

[3] C.-C. Chou and P.-T. Chung, "Development of cross-anchored dual-core self-centering braces for seismic resistance," *Journal of Constructional Steel Research*, vol. 101, pp. 19–32, 2014.

[4] AISC 341-16 (American Institute of Steel Construction), *Seismic Provisions for Structural Steel Buildings*, American Institute of Steel Construction, Chicago, IL, 2016.

[5] S.-H. Chao, C.-H. Kuo, H.-H. Huang, C.-C. Hsu, and J.-C. Jan, "Observed pulse-liked ground motion and rupture directivity effect in Taiwan ground motion dataset," in *Proceedings of International Conference in Commemoration of 20th Anniversary of the 1999 Chi-Chi Earthquake*, pp. 15–19, ChiChi20, Taipei, Taiwan, September 2019.

[6] Construction and Planning Agency Ministry of the Interior, *Seismic Design Specifications and Commentary of Buildings, Taiwan*, 2011.

[7] ASCE/SEI 41-17 (American Society of Civil Engineers), *Seismic Evaluation and Retrofit of Existing Buildings*, American Society of Civil Engineers, Reston, VA, 2017.

[8] S. Kiggins and C.-M. Uang, "Reducing residual drift of buckling-restrained braced frames as a dual system," *Engineering Structures*, vol. 28, no. 11, pp. 1525–1532, 2006.

[9] C.-C. Chou and Y.-C. Chen, "Development of steel dual-core self-centering braces: quasi-static cyclic tests and finite element analyses," *Earthquake Spectra*, vol. 31, no. 1, pp. 247–272, 2015.

[10] C.-C. Chou, P.-T. Chung, and Y.-T. Cheng, "Experimental evaluation of large-scale dual-core self-centering braces and sandwiched buckling-restrained braces," *Engineering Structures*, vol. 116, pp. 12–25, 2016.

[11] C.-C. Chou, C.-H. Hsiao, Z.-B. Chen, P.-T. Chung, and D.-H. Pham, "Seismic loading tests of full-scale two-story steel building frames with self-centering braces and buckling-restrained braces," *Thin-Walled Structures*, vol. 140, pp. 168–181, 2019.

[12] Y. Zhang and S. Zhu, "Seismic response control of building structures with superelastic shape memory alloy wire dampers," *Journal of Engineering Mechanics*, vol. 134, no. 3, pp. 240–251, 2008.

[13] F. Shi, O. E. Ozbulut, and Y. Zhou, "Influence of shape memory alloy brace design parameters on seismic performance of self-centering steel frame buildings," *Structural Control and Health Monitoring*, vol. 27, no. 1, Article ID e2462, 2020.

[14] L. Casagrande, C. Menna, D. Asprone, M. Ferraioli, and F. Auricchio, "Buildings," in *Shape Memory Alloy Engineering: For Aerospace, Structural, and Biomedical Applications*, pp. 689–729, Elsevier, 2nd edition, 2021.

[15] M. Ferraioli, A. Concilio, and C. Molitierno, "Seismic performance of a reinforced concrete building retrofitted with self-centering shape memory alloy braces," *Earthquake Engineering and Engineering Vibration*, vol. 21, no. 3, pp. 785–809, 2022.

[16] R. Tremblay, M. Lacerte, and C. Christopoulos, "Seismic response of multistory buildings with self-centering energy dissipative steel braces," *Journal of Structural Engineering*, vol. 134, no. 1, pp. 108–120, 2008.

[17] J. W. Baker, "Quantitative classification of near-fault ground motions using wavelet analysis," *Bulletin of the Seismological Society of America*, vol. 97, no. 5, pp. 1486–1501, 2007.

[18] M. H. Mohammadi, A. Massumi, and A. Meshkat-Dini, "Near-fault effects on RC buildings' demand in linear and nonlinear analyses," *Scientia Iranica*, vol. 26, no. 1, pp. 188–201, 2019.

[19] J. L. Gillie, A. Rodriguez-Marek, and C. McDaniel, "Strength reduction factors for near-fault forward-directivity ground motions," *Engineering Structures*, vol. 32, no. 1, pp. 273–285, 2010.

[20] H. Moniri, "Evaluation of seismic performance of reinforced concrete (RC) buildings under near-field earthquakes," *International Journal of Advanced Structural Engineering*, vol. 9, no. 1, pp. 13–25, 2017.

[21] C.-C. Chou, P. T. Chung, P. Nian, and Y. F. Liu, "High-rise reinforced concrete buildings retrofitted using steel double K-braced frame and one-sided shear strengthening schemes," in *12th National Conference in Earthquake Engineering*, No.10337, NCEE, Salt Lake City, UT, January 2022.

[22] C. Fang, Q. Zhong, W. Wang, S. Hu, and C. Qiu, "Peak and residual responses of steel moment-resisting and braced frames under pulse-like near-fault earthquakes," *Engineering Structures*, vol. 177, pp. 579–597, 2018.

[23] H. Krawinkler, B. Alavi, and F. Zareian, "Impact of near-fault pulses on engineering design," in *Directions in Strong Motion Instrumentation*, P. Gülkan and J. G. Anderson, Eds., vol. 58 of *Nato Science Series: IV: Earth and Environmental Sciences*, pp. 83–106, Springer, Dordrecht, 2005.

[24] Construction and Planning Agency Ministry of the Interior, "Design and Technique Specifications of Steel Structures for Buildings, Taiwan," 2007.

[25] ASCE/SEI 7-16 (American Society of Civil Engineers), *Minimum Design Loads for Buildings and Other Structures*, American Society of Civil Engineers, Reston, VA, 2017.

[26] AISC 341-22 (American Institute of Steel Construction), *Seismic Provisions for Structural Steel Buildings*, American Institute of Steel Construction, Chicago, IL, 2022.

[27] B.-Z. Lin, M.-C. Chuang, and K.-C. Tsai, "Object-oriented development and application of a nonlinear structural analysis framework," *Advances in Engineering Software*, vol. 40, no. 1, pp. 66–82, 2009.

[28] R. Allahabadi and G. H. Powell, *DRAIN-2DX User's Guide*, University of California, Berkeley, Report No. UCB/EERC-88/06, 1988.

[29] B. Z. Lin, Y. J. Yu, M. C. Chuang, and K. C. Tsai, *Platform of Inelastic Structural Analysis for 3D Systems, PISA3D Standard Edition R3.2 User's Manual*, National Center for Research on Earthquake Engineering, Taiwan, 2011.

[30] C.-C. Chou, J.-H. Liu, and D.-H. Pham, "Steel buckling-restrained braced frames with single and dual corner gusset connections: seismic tests and analyses," *Earthquake Engineering & Structural Dynamics*, vol. 41, no. 7, pp. 1137–1156, 2012.

[31] C.-C. Chou and C.-M. Uang, "A procedure for evaluating seismic energy demand of framed structures," *Earthquake Engineering & Structural Dynamics*, vol. 32, no. 2, pp. 229–244, 2003.

[32] M. Poursha, F. Khoshnoudian, and A. S. Moghadam, "A consecutive modal pushover procedure for estimating the

seismic demands of tall buildings," *Engineering Structures*, vol. 31, no. 2, pp. 591–599, 2009.

[33] H. Sucuoğlu and M. S. Günay, "Generalized force vectors for multi-mode pushover analysis," *Earthquake Engineering & Structural Dynamics*, vol. 40, no. 1, pp. 55–74, 2011.

[34] M. Kreslin and P. Fajfar, "The extended N2 method taking into account higher mode effects in elevation," *Earthquake Engineering & Structural Dynamics*, vol. 40, no. 14, pp. 1571–1589, 2011.

[35] M. Ferraioli, A. Lavino, and A. Mandara, "An adaptive capacity spectrum method for estimating seismic response of steel moment-resisting frames," *International Journal of Earthquake Engineering*, vol. 1, no. 2, pp. 47–60, 2016.

[36] Y. Liu and J. S. Kuang, "Spectrum-based pushover analysis for estimating seismic demand of tall buildings," *Bulletin of Earthquake Engineering*, vol. 15, no. 10, pp. 4193–4214, 2017.

[37] M. Ferraioli, "Multi-mode pushover procedure for deformation demand estimates of steel moment-resisting frames," *International Journal of Steel Structures*, vol. 17, no. 2, pp. 653–676, 2017.

[38] A. Y. Rahmani, N. Bourahla, R. Bento, and M. Badaoui, "Adaptive upper-bound pushover analysis for high-rise moment steel frames," *Structures*, vol. 20, pp. 912–923, 2019.

[39] T.-H. Lin and C.-C. Chou, "High-strength steel deep H-shaped and box columns under proposed near-fault and post-earthquake loadings," *Thin-Walled Structures*, vol. 172, Article ID 108892, 2022.

[40] C. Fang, Y. Ping, and Y. Chen, "Loading protocols for experimental seismic qualification of members in conventional and emerging steel frames," *Earthquake Engineering & Structural Dynamics*, vol. 49, no. 2, pp. 155–174, 2020.

[41] FEMA P-1050-1 Federal Emergency Management Agency, *NEHRP Recommended Seismic Provisions for New Buildings and Other Structures*, Building Seismic Safety Council, Washington, DC, Report No. FEMA P-1050-1, 2015.